IEEE Access
Multidisciplinary | Rapid Review | Open Access Journal

Received December 14, 2018, accepted December 24, 2018, date of publication January 31, 2019, date of current version February 22, 2019.

Digital Object Identifier 10.1109/ACCESS.2019.2895818

Isolation Transformer for 3-Port 3-Phase Dual-Active Bridge Converters in Medium Voltage Level

SEUNGHUN BAEK[1], (Member, IEEE), AND SUBHASHISH BHATTACHARYA[2], (Senior Member, IEEE)

[1]Department of Electrical Engineering, Kyungnam University, Changwon 51767, South Korea
[2]Department of Electrical and Computer Engineering, North Carolina State University, Raleigh, NC 27606, USA

Corresponding author: Subhashish Bhattacharya (sbhatta4@ncsu.edu)

This work was supported by the Kyungnam University Foundation Grant, 2017.

ABSTRACT In this paper, an isolation transformer with integrated filter inductances for three-phase three-port dual-active bridge (DAB) converters in the wye-wye-delta (Yyd) configuration is introduced and designed. A large number of ports and phases in the application necessarily requires a proportionally increased number of components, accessories, and connections. These additional parts induce significant losses and electromagnetic interference during high-frequency operations. Hence, fully manipulating the parasitic components, especially the leakage inductances of the transformer as the circuit element in the interconnected multi-port configuration, is a key to reduce the system's overall size and to improve its reliability. The proposed geometry and design method enables the full integration of a large number of otherwise bulky inductors to be included in the isolation transformers so that the latter function not only a step-up/down transformers but also as filter networks required for three-port DAB operations. The transformer is suitable for high-power and high step-up/down ratio dc-dc converters, which prefers a parallel combination of converters that share current, on the low-voltage side. The operating principles and steady-state analysis are presented with respect to power flow, and a three-winding shell-type isolation/filter transformer has been designed for a three-port three-phase Yyd DAB converter for solid state transformer applications. The finite element method simulations are used to validate the feasibility of the proposed approach. A prototype was fabricated and tested in an experimental setting.

INDEX TERMS Dual active bridge converter, three-winding transformer, solid state transformer.

I. INTRODUCTION

State-of-the-art power conversion applications linking grids and distributed sources, such as solid state transformer (SST) applications, tend to have a relatively low power rating compared to conventional utilities connected to a grid in the medium-voltage level [1]–[5]. One of the SST applications developed in support of the U.S Department of Energy, the Transformerless Intelligent Power Substation (TIPS) application, consists of a three-level neutral point clamped (NPC) converter on the high voltage (HV) side with paralleled 3-phase inverters in a high frequency six-step mode on the low voltage (LV) side [1]–[3]. An 11 kV DC signal from the 3-phase rectifier is stepped-down to 400 V DC through the DC-DC conversion stage, as indicated in Table 1. The specific operating condition requires that the power conversion systems to be electrically isolated and handle a high ratio of voltage to current. As a laboratory prototype for the DC-DC stage of TIPS, a three-level NPC converter on the HV side is replaced by 3-phase inverters on the LV side and a 3-port 3-phase wye-wye-delta (Yyd) DAB DC-DC converter is introduced, as shown in Fig. 1.

The 3-phase concept is applied to dual-active bridge (DAB) converters, which are used mostly in low voltage applications based on the wye-wye (Yy) connection. However, most distribution transformers in the medium voltage range belong in the vector group Yd11 (IEC60076-1) because there are always third-harmonic components. Therefore,

The associate editor coordinating the review of this manuscript and approving it for publication was Yuhao Liu.

TABLE 1. Specifications of the Lab. Prototype of TIPS application.

Freq.	V_{1dc}	V_{2dc}	Transformer connection	Control scheme
10kHz	5500V	400V	HV : wye LV1 : wye LV2 : delta	DAB Phase shift modulation

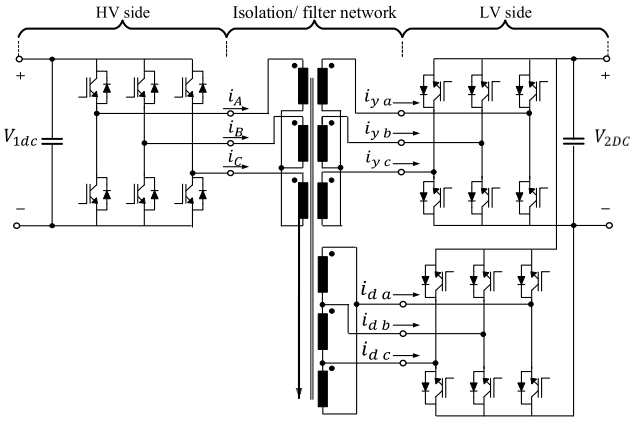

FIGURE 1. Configuration of 3-port 3-phase bidirectional DAB converter in Yyd connection.

a delta connection is preferred to provide a path for 3rd-harmonic current components in 3-phase systems. Conceptually, the same principles apply to the 3-port 3-phase isolated DAB converter for solid state transformer (SST) applications converting thousands of volts to secondary voltages.

The medium voltage on the HV side and high current on the LV side during high frequency switching operations makes the design of the DC-DC conversion stage challenging. In this topology, the 10 kHz switching operation at 5.5 kV on the HV side is handled by 15 kV SiC n-IGBTs (insulated-gate bipolar transistors) developed by Cree. The high current on the LV side during DAB operation is the largest source of system losses [6]; hence the parallel-connected converters share the current on the LV side and reduce losses and stresses in power devices. The operating principles used here are based on the phase shift modulation (PSM) scheme of a DAB converter, which mitigates stresses on power devices by using soft-switching (zero-voltage switching (ZVS)) [7].

Reduction of the size of the reactive components of the DC-DC stage is the key to realize a compact SST system. The filter network in the DC-DC stage in the topology is formed by a large number of isolation transformers and filter inductors. DAB operations require a certain amount of series inductance between converters, which includes leakage magnetic energy stored in the isolation transformers, to transfer a required range of power. Particularly, the high voltage to current ratio of the application requires the converters to have relatively large values of inductance, whose value is usually not in the range of the leakage inductance of conventional transformers. In many cases, the required filter inductance is realized by measuring the parasitic inductances of the conduction path of the circuit, which consist mainly of the leakage inductance of the isolation transformers, and then adding external inductors to make up the remaining value required. Therefore, the isolation transformers play a critical role in DAB operations for overall system performance and size.

The isolation transformers for the application DAB system we consider were built and tested with an additional nine inductors [8]. Not only are the transformers and inductors bulky, but significant oscillation occurs in the voltage and current waveforms during 10 kHz switching operations. Connections are significant sources of the parasitic components, electromagnetic (EM) interference, and losses in high frequency operations. As operating frequency and voltage increase, adding a part and its accessories requires an additional dedicated design effort. To circumvent these issues, the large number of filter inductors is removed by integrating filter inductors into the isolation transformers.

The isolation transformer has to provide a proper 3-port filter network to transfer power between the LV and HV sides of the converter. Bidirectional power flow between any two ports is equally possible in magnetically coupled windings. In order to obtain desirable power flows between ports without additional inductors, the leakage inductances have to be designed to form the desired filter network.

The desirable features and requirements of the filter network for the 3-port 3-phase isolated DAB converter are as follows:

1. Bidirectional power flow of the 3-port network should occur between the LV and HV sides (port 1 $\leftrightarrow$ port 2, and port 1 $\leftrightarrow$ port 3).
2. Soft-switching ZVS regions are maximized.
3. The circulating current between port 2 and 3 through the DC link on the LV side is minimized.
4. The filter inductances are fully integrated with the isolation transformers so that the large number of external inductors, connections, and accessories are eliminated.
5. Low profile geometry is preferred to make the system modular and to effectively handle thermal dissipation.

The geometry and configuration of the proposed isolation/filter transformer in this paper has a variety of advantages for 3-port 3-phase DAB converter applications. A shell-type planar shape is selected so that the magnetic fields are guided by high permeability magnetic cores and can be adjusted to the design values in an analytical manner. The leakage magnetic field between windings becomes predictable and adjustable by utilizing geometry and winding arrangement. The filter network is fully designed and integrated with the isolation transformers, and power flow is controlled between the LV and HV sides by applying the introduced method.

This paper also investigates the steady state circuit behavior of the 3-port 3-phase DAB converters of the TIPS system with the introduced isolation/filter transformer in Section II. The required filter network is integrated with isolation transformers by an analytical method using a

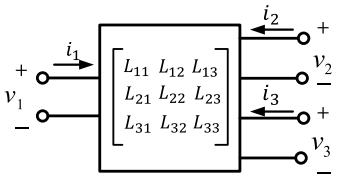

FIGURE 2. 3-port system with 3×3 inductance.

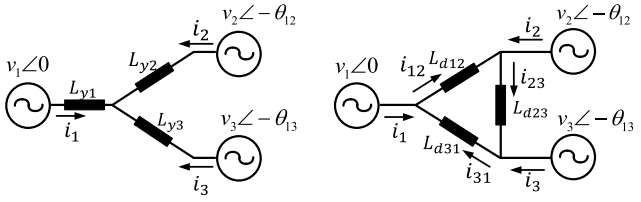

FIGURE 3. (a) Primary-referred wye-type equivalent circuit (b) Primary-referred delta-type equivalent circuit.

one-dimensional approximation in Section III. The analytical solutions of the 3-port 3-phase DAB operation based on the equivalent circuit model with terminal leakage inductances is presented and verified using finite element method (FEM) simulations in Section IV. The prototype isolation/filter transformer is fabricated and tested with a laboratory prototype to validate the operational principles and design method. The experimental results are presented to confirm the proposed approach and design method in Section V.

II. STEADY-STATE POWER FLOW IN 3-PORT 3-PHASE DAB CONVERTERS

A. FILTER NETWORK MODELS OF THE 3-PORT SYSTEM

It is meaningful to understand the system behavior with fundamental frequency components, which has a dominant impact on system performance and simplifies analysis in aid of vector notation. A port network is used for circuit analysis with terminals carrying equal and opposite currents. The 3-port system is represented by an impedance or admittance model when the system is a lossless and linear as shown in Fig 2.

The 3-port 3-phase DAB converters with a filter network can be seen as a 3-port system with the 3×3 impedance model. The effect of the capacitances and resistances of the power conversion system is ignored as a parasitic effect; hence, the impedance model can be seen as pure 3×3 inductance model in (1).

$$\begin{bmatrix} L_{11} & L_{12} & L_{13} \\ L_{21} & L_{22} & L_{23} \\ L_{31} & L_{32} & L_{33} \end{bmatrix} d/dt \begin{bmatrix} i_1 \\ i_2 \\ i_3 \end{bmatrix} = \begin{bmatrix} v_1 \\ v_2 \\ v_3 \end{bmatrix} \tag{1}$$

The 3-port 3-phase DAB DC-DC converter is simplified to a one-line diagram with three independent voltage sources and three lumped inductances in a wye or delta-type equivalent circuit, respectively [11], as shown in Fig. 3. The simplified circuit models are not theoretically perfect representations of the 3×3 inductance matrix [13], [14]. However, the wye or delta-type equivalent circuit and derivations are the accepted practice to represent three-winding transformers for circuit analysis in the industry, because the equivalent circuits represent the electrical behavior of three-winding transformers with an acceptable error, and the parameters are based on terminal leakage inductances, which are easily measurable.

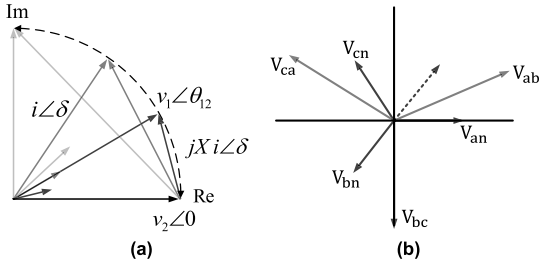

FIGURE 4. (a) Voltage and current vectors between ports of the Δ-type equivalent circuit (b) Voltage and current vectors in 3-phase system.

Two important operating principles are perceived through the phasor analysis of the delta-type equivalent circuit. Bidirectional power flow between any two ports is equally possible, and the direction is determined by the phase displacement in (2).

$$P_{ij} = \frac{V_i V_j \sin\theta_{ij}}{\omega L_{dij}}, \quad Q_{ij} = \frac{V_i(V_i - V_j\cos\theta_{ij})}{\omega L_{dij}} \tag{2}$$

The magnitude of the real and reactive power is determined by the magnitude of voltage, inductance values in the filter network, and the phase displacement. Note that two important system parameters in the PSM control scheme to determine the power flow of DAB; these are the control parameter (the phase shift 'θ_{ps}'), and the filter inductance values. The DC link voltages are fixed in the application but also are adjustable by the transformer turns ratio in practice. The real power is always zero when there is no phase displacement between voltages. However, reactive power circulates when the excited voltages are different, as seen defined in (2).

Considering the two voltage sources connected with a series inductor in Fig. 4(a), which is a branch of the delta-type equivalent circuit, the line current always lags v_1 and leads v_2 when the magnitude of the voltage vectors are is the same. During this operating condition, the power devices of leading bridges are turned on while the anti-parallel diode is conducting. The voltage seen from the power device is nearly zero during the switch-on transition, which is called zero-voltage switching (ZVS). ZVS is one of the essential properties of DAB converters to that make this topology suitable to for high-power and high frequency operations;. therefore, a suitable transformer turns ratio and control strategy should be determined in order to maximize the range of ZVS in the operation region.

B. POWER CONTROL STERATEGY FOR 3-PORT 3-PHASE DAB CONVERTER IN Yyd CONFIGURATION

The turns-ratio of the transformer provides a degree of freedom when choosing the buck-boost gain of the DAB converter. The buck-boost conversion ratio changes the oper-

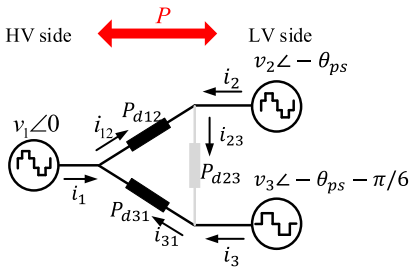

FIGURE 5. The desirable filter network in one-line diagram for the 3-port 3-phase converter.

ation and soft-switching region of the DAB converter; hence, the turns ratio of the isolation transformer significantly influences overall system performance and efficiency.

Power must be transferred between the LV side and HV side of the converter, i.e., between port 1–port 2 and port 1–port 3. The buck-boost gain of the DAB converter 'd' is preferred to be unity from the HV side to the LV side so that the magnitude of the voltage of each port is the same, which will maximize the ZVS soft-switching region. In other words, the turns ratio among the three windings is preferred to be equal to the voltage ratio among the three voltage sources.

The wye-delta connection in a 3-phase system inherently has a magnitude change of $\sqrt{3}$ and phase displacement of $\pi/6$ (30°), as shown in Fig. 4(b); hence, the mismatch has to be compensated for by active switching control of the bridge and by the turns ratio of the windings. In order to ensure that there is no real power circulating within the LV side through the DC link, the phase shift angle between port 1 and port 3 is always another $\pi/6$ higher than the control variable 'θ_{ps}'. Hence, the turns ratios between port 1, port 2, and port 3 in a Yyd configuration should be $55{:}4{:}4\sqrt{3}\,e^{j\pi/6}$ to consider the factor of $\sqrt{3}\,e^{j\pi/6}$ in the Yd connection on the LV side.

Furthermore, the filter inductance L_{d13} is inversely proportional to the magnitude of the circulating current i_{23}. Hence, L_{d13} in the delta-type equivalent circuit is preferred to be large and ideally ignorable in the parallel connection. Considering these points, Fig. 5 shows the most desirable configuration in one-line diagram form.

C. OPERATIONS OF 3-PORT 3-PHASE DAB CONVERTER IN Yyd CONFIGURATION

The three voltage sources in Fig. 5 are replaced by three 3-phase inverters in high frequency six-step mode in the real system. The phase voltages generated by six-step 3-phase inverters in wye and delta connections are multi-level square waveforms, as shown in Fig. 6. Phase shift modulation is applied using the control variable '$\boldsymbol{\theta_{ps}}$' with gating signals having a duty ratio of 0.5. From Fig. 6, the actual voltage $\boldsymbol{v_1}$, $\boldsymbol{v_2}$, $\boldsymbol{v_3}$ and current $\boldsymbol{i_{12}}$, $\boldsymbol{i_{23}}$, $\boldsymbol{i_{31}}$ waveforms in the delta-type equivalent circuit are calculated and shown for the Yy and Yd connections, respectively [9], [10]. Windings 1, 2, and 3 have the number of turns set as 55:4:7, and the additional phase displacement of $\pi/6$ is applied between port 1 and 3.

The fundamental and harmonic components of the phase voltage of port 2 in the wye connection are represented in sine series form in (3).

$$v_{2an} = V_{2dc}\frac{2}{\pi}\left(\sin(\omega t) + \frac{1}{5}\sin(5\omega t) + \frac{1}{7}\cos(7\omega t) + \frac{1}{11}\cos(11\omega t)\,..\right) \quad (3)$$

The fundamental and harmonic components of the phase voltage of port 3 in the delta connection with additional phase shift $\pi/6$ are derived as

$$v_{3ab} = \sqrt{3}V_{2dc}\frac{2}{\pi}\left(\sin(\omega t) - \frac{1}{5}\sin(5\omega t) - \frac{1}{7}\sin(7\omega t) + \frac{1}{11}\sin(11\omega t)\,..\right). \quad (4)$$

Hence, the electromotive force on inductance L_{23} referred to the winding of port 2 is given by (5) considering the turns ratio of $\sqrt{3}$.

$$EMF_{L_{23}} = V_{2dc}\frac{4}{\pi}\left(\frac{1}{5}\cos(5\omega t) + \frac{1}{7}\cos(7\omega t) + \frac{1}{17}\cos(5\omega t) + \frac{1}{19}\cos(7\omega t)\,..\right) \quad (5)$$

The fundamental frequency components of the induced current flow between winding 2 and winding 3 are cancelled out, and the 5th, 7th, 17th, 19th, etc. elements remain, which cause circulating current and carry reactive power through the DC link on the LV side.

The amount of power transfer between ports can be derived from the actual voltage and current waveforms. The power

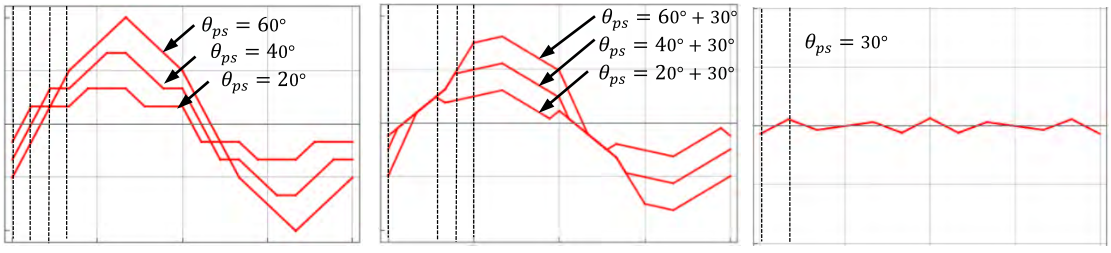

FIGURE 6. Phase current waveforms generated by 3-port 3-phase DAB converter in Yyd connection. (a) i_{12} (port 1→port 2, Yy). (b) $-i_{31}$ (port 1→port 3, Yd). (c) i_{23} (port 2→port 3, Yd).

transfer from port 1 to port 2 is derived as

$$\begin{cases} P_{Yy1} = \dfrac{dV_{1dc}^2\left(4\pi - 3\theta_{ps}\right)\theta_{ps}}{6L_{d12}\pi\omega}, & \left(0 \le \theta_{ps} \le \dfrac{\pi}{3}\right) \\ P_{Yy2} = \dfrac{dV_{1dc}^2\left(18\pi\theta_{ps} - \pi^2 - 18\theta_{ps}^2\right)}{18L_{d12}\pi\omega}, & \left(\dfrac{\pi}{3} \le \theta_{ps} \le \dfrac{\pi}{2}\right) \end{cases} \tag{6}$$

Considering the additional phase displacement of $\pi/6$, the power transfer from port 1 to port 3 is derived as,

$$\begin{cases} P_{Yd1} = \dfrac{dV_{1dc}^2\left(6(\theta_{ps} + \pi/6) - \pi\right)}{6\sqrt{3}L_{d13}\omega}, & \left(0 \le \theta_{ps} \le \dfrac{\pi}{6}\right) \\ P_{Yd2} = \dfrac{dV_{1dc}^2\left(12\pi\left(\theta_{ps} + \pi/6\right) - 2\pi^2 - 9(\theta_{ps} + \pi/6)^2\right)}{6\sqrt{3}L_{d13}\pi\omega}, & \left(\dfrac{\pi}{6} \le \theta_{ps} \le \dfrac{\pi}{2}\right) \end{cases} \tag{7}$$

Because the power transfer between port 2 and port 3 is always zero, the total power transfer from the HV side to the LV side is the sum of (6) and (7).

$$\begin{cases} P_{Yyd1} = P_{Yy1} + P_{Yd1}, & \left(0 \le \theta_{ps} \le \dfrac{\pi}{6}\right) \\ P_{Yyd2} = P_{Yy1} + P_{Yd2}, & \left(\dfrac{\pi}{6} \le \theta_{ps} \le \dfrac{\pi}{3}\right) \\ P_{Yyd3} = P_{Yy2} + P_{Yd2}, & \left(\dfrac{\pi}{3} \le \theta_{ps} \le \dfrac{\pi}{2}\right) \end{cases} \tag{8}$$

If $L_{d12} \cong L_{d13}$ is assumed, three equations are derived with respect to load conditions, given by (9), as shown at the bottom of the next page.

III. DESIGN OF THE FILTER NETWORK FOR 3-PORT 3-PHASE DAB CONVERTERS

A. GEOMETRIC INTERPRETATION WITH TERMINAL LEAKAGE INDUCTANCES OF 3-WINDING TRANSFORMERS

The filter network is determined by the geometrical information, winding arrangement, and the characteristics of the materials. A 1-dimentional approximation is used to achieve the aforementioned desirable features. Finally, 3-dimensional FEM models are used to validate the design as a post-process. First, the geometry of the magnetic cores must be symmetric and shielded by high permeability material in order to effectively guide the magnetic flux path. The shell-type configuration confines the leakage magnetic flux in the window area in uniform manner, as shown in Fig. 7. The planar shape reduces a portion of the parasitic effect from the edges and increases the accuracy of the 1-dimensional calculations.

A variety of advantages applicable to planar magnetics including good thermal characteristics and modular capability is known in the literature [12]. A trapezoidal shape of magnetic field intensity is formed in the window area when the current in the winding is evenly distributed in a sequential manner, as shown in Fig. 7. The stored magnetic energy in the window area is

$$E_{tij} = \frac{1}{2}P_{tij}i^2 = l\int_0^w H(x)dx, \tag{10}$$

where 'l' is the length of the core in the z direction.

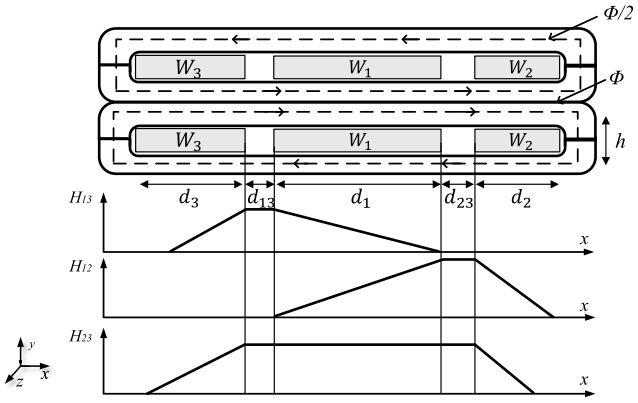

FIGURE 7. 3-winding shell-type transformer and trapezoidal leakage magnetic field intensity (H) distribution in window area.

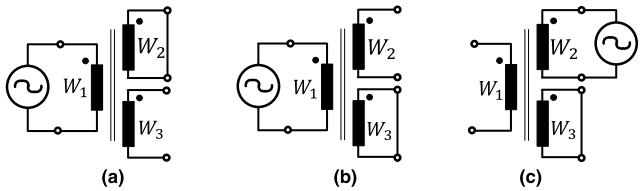

FIGURE 8. Terminal leakage inductance measurements. (a) L_{t12} ($v_2 = 0$, $i_3 = 0$). (b) L_{t13}, $v_3 = 0$, $i_2 = 0$. (c) L_{t23}, $v_3 = 0$, $i_i = 0$.

Terminal leakage inductances L_t are meaningful and measurable parameters of an isolation transformer in practice. The terminal leakage inductances are measured using two windings at a time by shorting the relevant winding and opening the last winding, as shown in Fig. 8. The permeance, 'P', a measure of the magnetic flux for one turn, is used instead of inductance 'L' in the following calculations.

The terminal leakage permeance is calculated from the trapezoidal magnetic flux distribution when the current in the winding is evenly distributed in sequential manner, as expressed in (11).

$$\begin{cases} P_{t12} = (d_1 + d_2 + 3d_{12})\,k \\ P_{t31} = (d_1 + d_3 + 3d_{13})k \\ P_{t23} = (3d_1 + d_2 + d_3 + 3d_{12} + 3d_{13})k \end{cases} \tag{11}$$

Here $k = \frac{\mu_o l}{3h}$ $P_{tij} = P_{yi} + P_{yj}$, $(L_{tij} = N_i^2 P_{tij})$

Hence, the circuit element of wye and delta-type equivalent circuit is represented by geometrical parameters in (12) and (13), as shown at the bottom of the next page, respectively.

The terminal permeance values in the wye/ delta equivalent circuit models are not mathematically consistent. The equivalent model of mutually-coupled inductors is compatible with terminal permeance measurements, and hence is applied in Fig. 9. The equivalent circuit is represented by the impedance matrix including the magnetic coupling $M = -P_{y1}$ in (14).

$$\begin{bmatrix} P_{t12} & P_{y1} \\ P_{y1} & P_{t13} \end{bmatrix} d/dt \begin{bmatrix} i_2 \\ i_3 \end{bmatrix} = \begin{bmatrix} v_{21} \\ v_{31} \end{bmatrix} \tag{14}$$

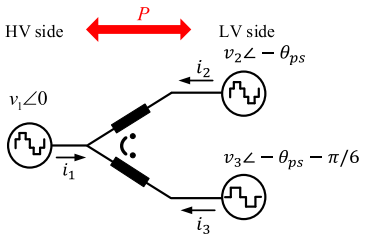

FIGURE 9. Equivalent circuit model of a 3-winding transformer.

The mutually coupled current does not go into port 1, as is case for circulating current i_{23} in the delta-type equivalent circuit. Note that all permeances are proportional to 'k' and the final permeance values will be double, considering the return path of shell-type cores.

B. FILTER INDUCTANCE INTERGRATION OF A 3-WINDING PLANAR TRANSFORMER FOR A Yyd 3-PORT 3-PHASE DC-DC CONVERTER

The power flows between ports 1 and 2 and between ports 1 and 3 are determined by the series permeances and control parameter θ_{ps}. P_{d12} and P_{d31} are preferred to be similar values to share current evenly in paralleled bridges, and are required to be within a certain range to transfer a specific amount of power. Hence, winding 1 in the middle between windings 2 and 3 is used as the isolation transformer on the HV side and windings 2 and 3 are used for the windings of the parallel-connected inverters on the LV side. The coupling M is relatively weak based on the geometry, and provides no contribution to real power flow in the application. Hence, the desirable filter network with two permeance elements, P_{t12} and P_{t31}, is reasonable.

The shell-type planar transformer has a predictable magnetic path, while the leakage inductance values can be amplified by shortening the leakage magnetic path in the window area. The height to length ratio of the planar shape adjusts the permeance values. The dimensions l, h, d are selected to produce the inductance values that DAB operation requires. The symmetric configuration produces similar terminal permeances between ports 1 and 2 and between ports 1 and 3. This winding arrangement is beneficial for balancing current sharing on the two bridges connected in parallel. Therefore, the proposed geometry and design method for the isolation transformer allows us to integrate and replace the large number of bulky inductors required for DAB operations while achieving the intended power flow.

The prototype transformer was designed with a width/height ratio of 21.7 to achieve the two similar terminal inductances L_{t12} and L_{t31} of 12 mH referred to the HV side. The specifications and dimensions of the magnetic cores are listed in Table 2. Computer-aided drawings of the prototype were used for fabrication. The FEM analysis structure is illustrated in Fig. 10. There are a variety of design factors affecting the magnetics design; therefore, further optimization is expected by conducting parametric studies.

IV. DESIGN VALIDATION USING FEM

A. FEM MAGNETOSTATIC SOLUTIONS

The exact behavior of the transformer during complex converter operations in three dimensions was simulated with the aid of FEM tools. Ansys Maxwell3D magnetostatic solvers

$$\begin{cases} P_{Yyd1} \cong \dfrac{dV_{1dc}^2\left(2(2+\sqrt{3})\,\pi - 3\theta_{ps}\right)\theta_{ps}}{6L\pi\omega}, & \left(0 \le \theta_{ps} \le \dfrac{\pi}{6}\right) \\ P_{Yyd2} \cong \dfrac{dV_{1dc}^2(-\sqrt{3}\pi^2 + 12\left(4+3\sqrt{3}\right)\pi\theta_{ps} - 36(1+\sqrt{3})\theta_{ps}^2)}{72L\pi\omega}, & \left(\dfrac{\pi}{6} \le \theta_{ps} \le \dfrac{\pi}{3}\right) \\ P_{Yyd3} \cong \dfrac{-dV_{1dc}^2(\left(4+3\sqrt{3}\right)\pi^2 + 36\left(2+\sqrt{3}\right)\pi\theta_{ps} - 36(2+\sqrt{3})\theta_{ps}^2)}{72L\pi\omega}, & \left(\dfrac{\pi}{3} \le \theta_{ps} \le \dfrac{\pi}{2}\right) \end{cases} \tag{9}$$

$$\begin{cases} P_{y1} = -\dfrac{d_1}{2}k \\ P_{y2} = (\dfrac{3}{2}d_1 + d_2 + 3d_{12})k \\ P_{y3} = (\dfrac{3}{2}d_1 + d_3 + 3d_{13})k \end{cases} \tag{12}$$

$$\begin{cases} P_{d12} = \dfrac{\left(3d_1^2 + 4\left(3d_{12}+d_2\right)\left(3d_{13}+d_3\right) + 4d_1\left(3d_{12}+3d_{13}+d_2+d_3\right)\right)k}{6d_1 + 4(3d_{13}+d_3)} \\ P_{d23} = \dfrac{-3d_1^2k - 4\left(3d_{12}+d_2\right)\left(3d_{13}+d_3\right)k - 4d_1\left(3d_{12}+3d_{13}+d_2+d_3\right)k}{2d_1} \\ P_{d31} = \dfrac{\left(3d_1^2 + 4\left(3d_{12}+d_2\right)\left(3d_{13}+d_3\right) + 4d_1\left(3d_{12}+3d_{13}+d_2+d_3\right)\right)k}{6d_1 + 4(3d_{12}+d_2)} \end{cases} \tag{13}$$

TABLE 2. Prototype dimensions [mm].

A	F	B	G	E	D
150	130	26	6	10	50
d_1	d_2	d_3	d_{12}	d_{13}	l	h
59	19	32	6	7	600	6

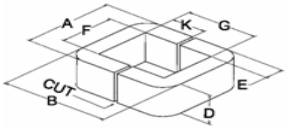

TABLE 3. Terminal permeances and inductances referred to HV side.

	Calculation	3D FEM	Measurement
$P_{t\,12}$ [uH]	4.02	4.13	
$P_{t\,31}$ [uH]	4.69	4.77	
$P_{t\,23}$ [uH]	11.18	11.16	
$L_{t\,12}$ [mH]	12.16	12.49	@10kHz, 11.3
$L_{t\,12}$ [mH]	14.19	14.42	@10kHz, 12.5
$L_{t\,23}$ [mH]	33.83	33.77	@10kHz, 23.3

were used to extract terminal inductances. The geometry and specifications in Table 1 and Table 2 were used. Half of the model was drawn by setting a symmetric boundary condition to reduce computational load and time, as shown in Fig. 10(b). The size of the mesh of the magnetic cores on the MC1 was limited to within 1 mm, which is 1/150 of the width of the cores, to ensure the accuracy of curves and gaps. Three core sections, CS1, CS2, and CS3, were defined and used to calculate the magnetic field. The measurement conditions of terminal permeances are set by exciting currents on two windings in the opposite direction. The static magnetic field distributions and mesh sizes for each measurement are shown in Fig. 11. The magnetic fields are guided by high permeability magnetic cores and the magnetic field intensity is confined in the window area in a uniform manner, as designed.

This laboratory prototype of the 3-winding transformer for a 5.5 kV to 400 V DC-DC stage is designed for TIPS application, and results are shown in Fig. 12. Nanocrystalline magnetic cores were customized to operate at 10 kHz with high efficiency. Litz wires were used to reduce eddy and proximity effects on the windings. The bobbin is made of Teflon with 5.5 kV insulation. The calculated and measured permeance and inductance values from the prototype are compared in Table 3. The terminal leakage inductances were measured by an Agilent 4294A. Both the FEM results in three dimensions and analytical calculation results show good agreement. The measured values are reasonably within the expected range considering the imperfections of the manufacturing process and material properties. The measured L_{t23} value is approximately 70% of the FEM result and does not contribute to real power transfer.

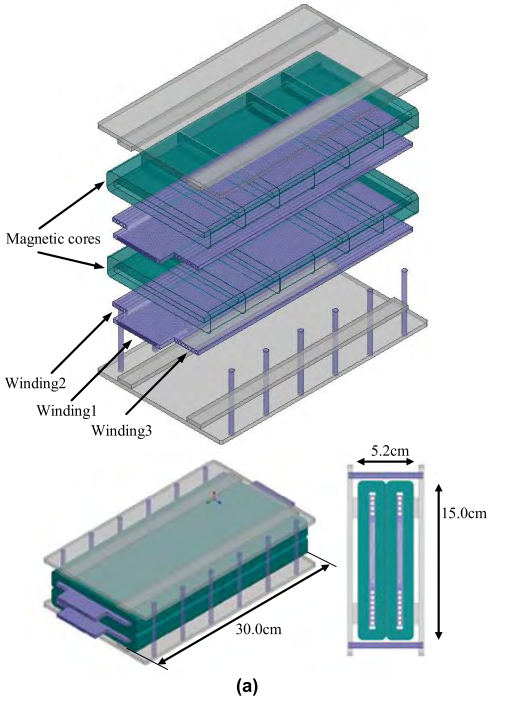

FIGURE 10. (a) CAD drawing of isolation/ filter transformer for 3-port 3-phase DC-DC converter in Yyd configuration (b) 3D FEM setup.

B. FEM TRANSIENT SOLUTIONS

The operational principles and analysis with the proposed method are verified by a FEM transient solver. The same drawings and setups for the magnetostatic solver are applied to the Ansys Maxwell3D transient solver. The phase voltages are directly applied to transformer windings without additional inductances. Hence, the magnetic energy stored by line currents during DAB operation is solely due to the leakage inductances of the transformer. The phase voltages and phase currents referred to the HV side are shown in Fig. 13. The average values of the magnetic field over the cross sectional areas, B_{avg_CS1}, B_{avg_CS2}, and B_{avg_CS3} are calculated based on (15).

$$B_{avg} = \frac{1}{A_{CS}} \int_{A_{CS}} \vec{B} \cdot \vec{n} dA \tag{15}$$

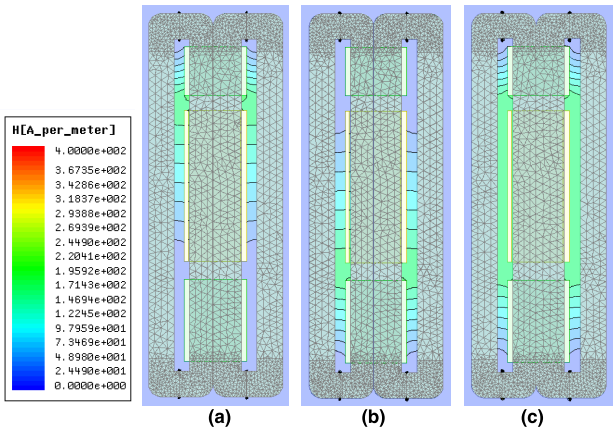

FIGURE 11. H-field distributions (a) P_{t12} with excitation of 1A (b) P_{t31} with excitation of 1A (c) P_{t23} with excitation of 1A.

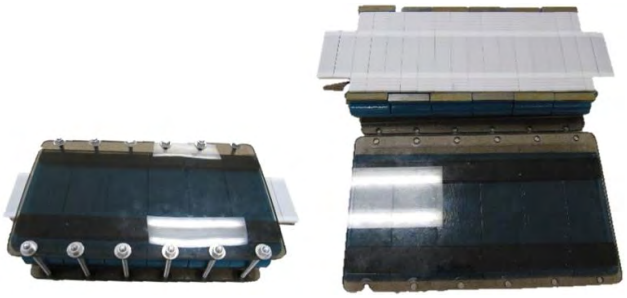

FIGURE 12. Prototype of isolation/filter transformer for 3-Port 3-phase DC-DC converter in Yyd connection.

Note that the location of $CS1$ on the x axis is in the middle of winding 1, and $CS2$ and $CS3$ are located between windings. B_{avg_CS1} is almost constant with time regardless of change in load conditions (Fig. 13), which indicates that B_{avg_CS1} is not affected by line currents. The location of $CS1$ is such that the two leakage magnetic paths are balanced and cancel each other; thus, B_{avg_CS1} can be used as an indication of magnetic fields for mutual coupling. When θ_{ps} is 20° under light load conditions, B_{avg_CS2} and B_{avg_CS3} are almost the same as B_{avg_CS1} in Fig. 13(a).

The magnetic field distribution in the magnetic cores under heavy load conditions with $\theta_{ps} = 60°$ is shown in Fig. 13(c). The line currents reach peak values at approximately $35us$ with $\theta_{ps} = 60°$ and B_{avg_CS2} and B_{avg_CS3} are almost zero because the magnetic field is almost horizontal to the cross sectional area owing to the strong magnetic field induced by line currents along the leakage paths in Fig. 14. The line current at $10us$ is close to zero in Fig. 13(c), where B_{avg_CS1}, B_{avg_CS2}, and B_{avg_CS3} cross over, indicating that the magnetic field induced by line currents along the leakage paths does not exist. Hence, the magnetic field distribution shown in the plot at $10us$ in Fig. 14 is mainly formed by mutual coupling and the magnetic fields in the cores are well aligned in a uniform manner.

The amount of power transfer from each winding per phase is calculated by the phase current and voltage waveforms

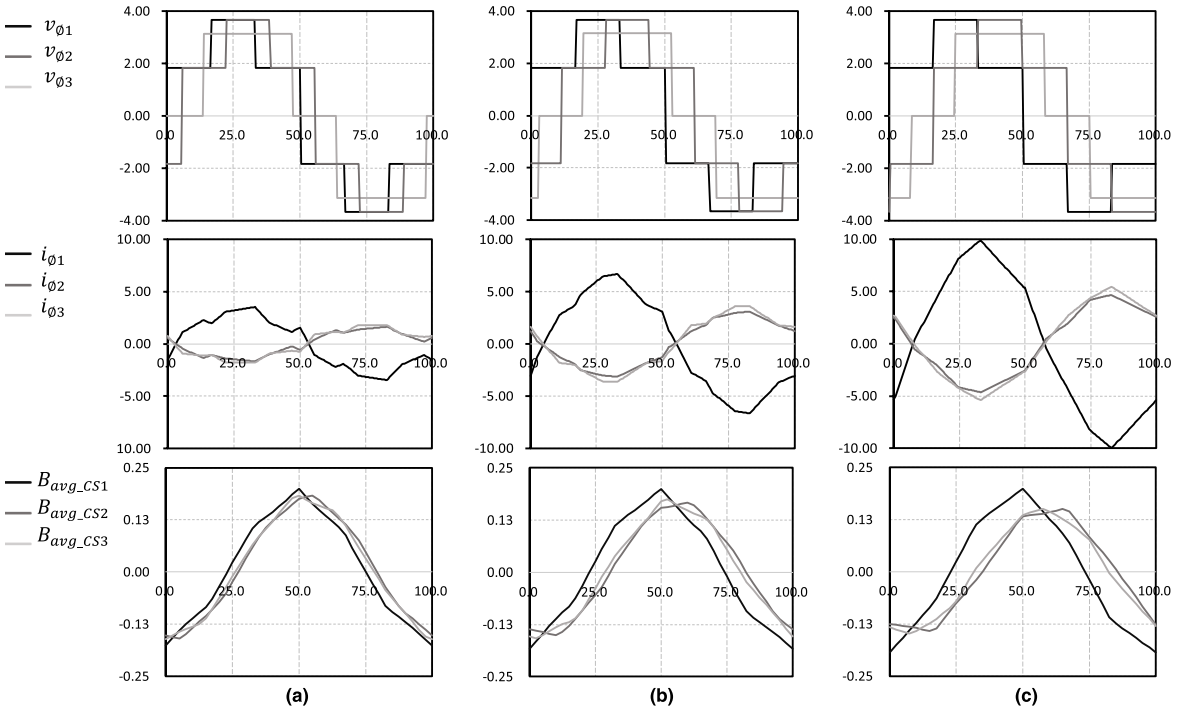

FIGURE 13. 3D FEM transient solutions – waveforms in time (time step = 0.5us). (a) $\theta_{ps} = 20°$. (b) $\theta_{ps} = 40°$. (c) $\theta_{ps} = 60°$.

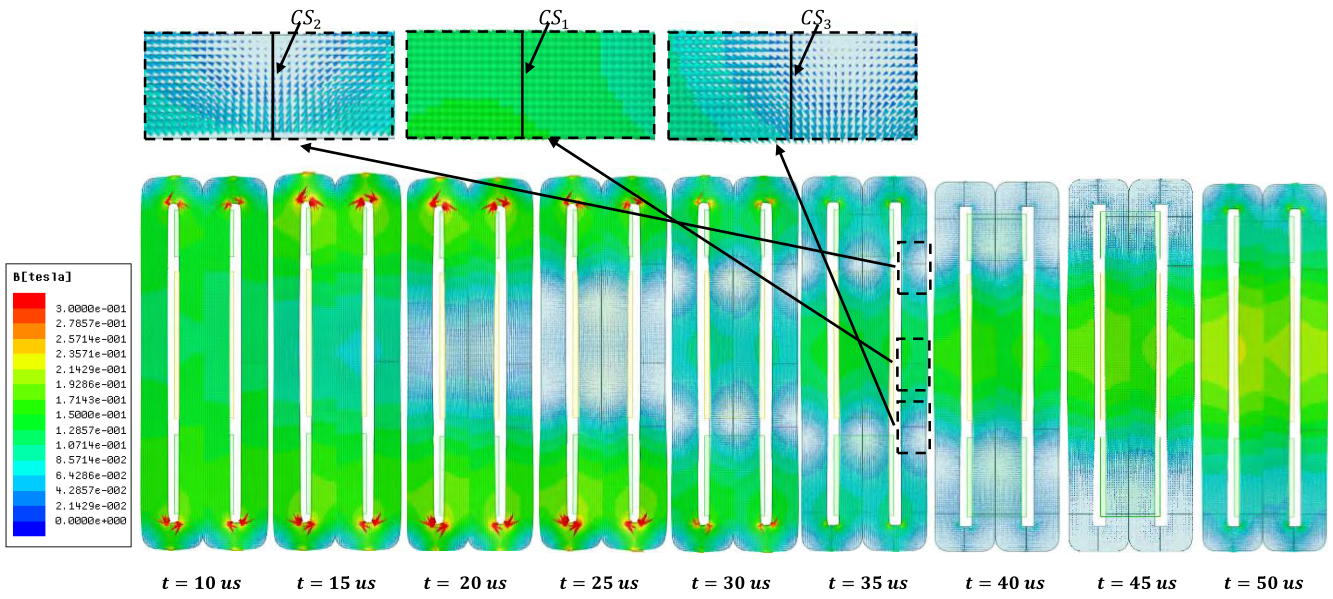

FIGURE 14. B-field distributions with time on the cross sectional view, $\theta_{ps} = 60°$, power: 14.21kW.

TABLE 4. Power delivery calculation results per phase.

θ_{ps}		Winding 1 (port 1)	Winding 2 (port 2)	Winding 3 (port 3)
20°	Calculation	5.09kW	-2.81kW	-2.28kW
	3D FEM	5.51kW	-2.98kW	-2.45kW
40°	Calculation	9.56kW	-5.10kW	-4.46kW
	3D FEM	10.46kW	-5.43kW	-4.88kW
60°	Calculation	12.88kW	-6.90kW	-5.98kW
	3D FEM	14.21kW	-7.38kW	-6.56kW

from 3D FEM transient solutions using (16).

$$\frac{1}{T}\int_0^T v \cdot idt \tag{16}$$

The calculation results by the FEM transient solver are compared to the analytical solutions in Table 4. The sign of the power on each port indicates the direction of power flow. The amount of power on the LV side is evenly distributed on each branch and transferred to the HV side. Approximately 14.21 kW per phase is transferred between HV and LV sides with a phase shift of 60°.

There are local magnetic field congestions near the edges; however most core regions are in the 0.4 T range of the peak to peak value. The nonlinear BH curve of nanocrystalline cores is applied to FEM simulations; however the results do not produce considerable changes because the operating conditions are well within the linear region of the core material which has its saturation point around 1.2T.

The magnetic field induced by line currents in the leakage paths can generate additional losses near $CS2$ and $CS3$ in laminated structure, which become orthogonal to the lamination and induce eddy currents. Hence, further study in efficiency need to be done in case that cores in laminated structure are applied.

TABLE 5. Test conditions.

Freq	V_{1dc}	V_{2dc}	Transformer Connection (turns)	Control scheme
10kHz	300V	300V	Port 1: wye (4) Port 2: wye (4) Port 3: delta (7)	DAB Phase shift modulation

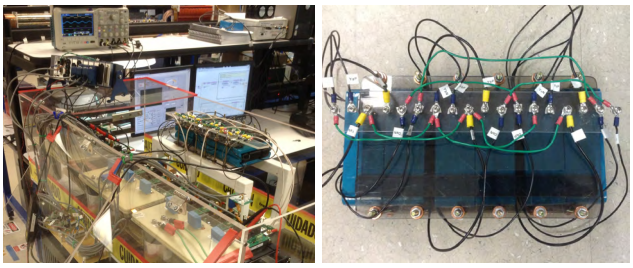

(a) (b)

FIGURE 15. (a) Test set-up for the 3-Port 3-phase DC-DC converter in Yyd connection (b) the scale-down prototype transformers.

V. EXPERIMENTAL RESULTS

To validate the operational principles and power flows, scaled-down experiments were conducted with three inverters in six-step mode, as given in in Table 5. Three three-winding transformers were built at one-third scale and were connected without additional inductors. DC-link voltages on both sides were set to 300 V and phase shift modulation was applied at a fixed frequency of 10 kHz with turns ratios of $1 : 1 : \sqrt{3}$ for the setup shown in Fig. 15. The phase shift, θ_{ps}, was applied between the HV and LV sides and the delta-connected

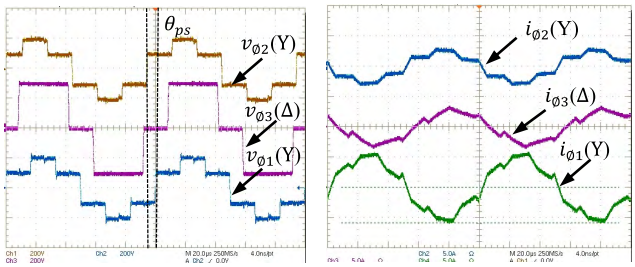

FIGURE 16. Waveforms on each winding, $\theta_{ps} = 20°$ (500V/Div, 5A/Div, 20us/Div).

inverter had an additional phase displacement of $\pi/6$. Waveforms with a phase shift of 20° are shown in Fig. 16. There were no oscillation issues, and the expected waveforms were achieved.

VI. CONCLUSIONS

In this paper, the 3-winding shell-type isolation/filter transformer has been designed for the 3-port 3-phase DAB converter in Yyd connection for SST applications. The isolation transformer introduced in this paper functions not only as an isolation transformer but also as inductive filters for 3-port filter network. The power flow characteristics of the converter operation is analyzed through equivalent circuit model with terminal leakage inductances. The desirable power flows between the three ports of the converter topology are obtained by manipulating the isolation transformer with a full integration of filter network. The proposed design and analysis of the isolation/filter transformer is verified by FEM simulations. The operation principles and the feasibility of isolation transformer as a filter network for the 3-port 3-phase DC-DC converter in Yyd connection is proven by experimental results.

REFERENCES

[1] S. Bhattacharya, "Transforming the transformer," *IEEE Spectr.*, vol. 54, no. 7, pp. 38–43, Jul. 2017.

[2] K. Mainali *et al.*, "A transformerless intelligent power substation: A three-phase SST enabled by a 15-kV SiC IGBT," *IEEE Power Electron. Mag.*, vol. 2, no. 3, pp. 31–43, Sep. 2015.

[3] K. Hatua, S. Dutta, A. Tripathi, S. Baek, G. Karimi, and S. Bhattacharya, "Transformer less intelligent power substation design with 15kV SiC IGBT for grid interconnection," in *Proc. Energy Convers. Congr. Expo. (ECCE)*, 2011, pp. 4225–4232.

[4] J. W. Kolar and J. E. Huber, "Solid-state transformers key design challenges, applicability, and future concepts," in *Proc. 17th Int. Conf. Power Electron. Motion Control (PEMC)*, Varna, Bulgaria, Sep. 2016, p. 26.

[5] G. Wang *et al.*, "Design and hardware implementation of Gen-1 silicon based solid state transformer," in *Proc. 26th Annu. IEEE Appl. Power Electron. Conf. Expo. (APEC)*, Mar. 2011, pp. 1344–1349.

[6] F. Krismer and J. W. Kolar, "Accurate power loss model derivation of a high-current dual active bridge converter for an automotive application," *IEEE Trans. Ind. Electron.*, vol. 57, no. 3, pp. 881–891, Mar. 2010.

[7] R. W. A. A. De Doncker, D. M. Divan, and M. H. Kheraluwala, "A three-phase soft-switched high-power-density DC/DC converter for high-power applications," *IEEE Trans. Ind. Appl.*, vol. 27, no. 1, pp. 63–73, Jan. 1991.

[8] K. Mainali, A. Tripathi, D. C. Patel, S. Bhattacharya, and T. Challita, "Design, measurement and equivalent circuit synthesis of high power HF transformer for three-phase composite dual active bridge topology," in *Proc. IEEE Appl. Power Electron. Conf. Expo. (APEC)*, Mar. 2014, pp. 342–349.

[9] S. Baek, S. Roy, S. Bhattacharya, and S. Kim, "Power flow analysis for 3-port 3-phase dual active bridge DC/DC converter and design validation using high frequency planar transformer," in *Proc. IEEE Energy Convers. Congr. Expo. (ECCE)*, Sep. 2013, pp. 388–395.

[10] N. H. Baars, J. Everts, C. G. E. Wijnands, and E. A. Lomonova, "Performance evaluation of a three-phase dual active bridge DC–DC converter with different transformer winding configurations," *IEEE Trans. Power Electron.*, vol. 31, no. 10, pp. 6814–6823, Oct. 2016.

[11] C. Zhao, S. D. Round, and J. W. Kolar, "An isolated three-port bidirectional DC-DC converter with decoupled power flow management," *IEEE Trans. Power Electron.*, vol. 23, no. 5, pp. 2443–2453, Sep. 2008.

[12] Z. Ouyang and M. A. E. Andersen, "Overview of planar magnetic technology—Fundamental properties," *IEEE Trans. Power Electron.*, vol. 29, no. 9, pp. 4888–4900, Sep. 2014.

[13] F. De Leon and J. A. Martinez, "Dual three-winding transformer equivalent circuit matching leakage measurements," *IEEE Trans. Power Del.*, vol. 24, no. 1, pp. 160–168, Jan. 2009.

[14] P. S. S. Holenarsipur, N. Mohan, V. D. Albertson, and J. Cristofersen, "Avoiding the use of negative inductances and resistances in modeling three-winding transformers for computer simulations," in *Proc. IEEE Power Eng, Soc. Winter Meeting*, New York, NY, USA, Jan. 1999, pp. 1025–1030.

[15] Y.-M. Chen, Y.-C. Liu, and F.-Y. Wu, "Multi-input DC/DC converter based on the multiwinding transformer for renewable energy applications," *IEEE Trans. Ind. Appl.*, vol. 38, no. 4, pp. 1096–1104, Jul. 2002.

[16] H. Plesko, J. Biela, J. Luomi, and J. W. Kolar, "Novel concepts for integrating the electric drive and auxiliary DC–DC converter for hybrid vehicles," *IEEE Trans. Power Electron.*, vol. 23, no. 6, pp. 3025–3034, Nov. 2008.

SEUNGHUN BAEK (M'14) received the dual B.S. degree from Ajou University, Suwon, South Korea, and from the Illinois Institute of Technology, Chicago, IL, USA, in 2007, and the M.S. and Ph.D. degrees from North Carolina State University, Raleigh, NC, USA, in 2009 and 2014, respectively, all in electrical and computer engineering. He was with Enphase Energy, Inc., Petaluma, CA, USA, from 2014 to 2017, and joined Kyungnam University, Changwon, South Korea, in 2017, where he is currently an Assistant Professor. His research interests include high-frequency converters and mangetics, solid-state transformers, renewable energy, and smart-grid applications.

SUBHASHISH BHATTACHARYA (M'85–SM'13) received the B.E. degree from IIT Roorkee, Roorkee, India, the M.E. degree from the Indian Institute of Science, Bengaluru, India, and the Ph.D. degree from the University of Wisconsin–Madison, Madison, WI, USA, in 2003, all in electrical engineering. He was with the FACTS and Power Quality Division, Westinghouse/Siemens Power T&D, from 1998 to 2005. In 2005, he joined the Department of Electrical and Computer Engineering, North Carolina State University, Raleigh, NC, USA, where he is currently a Duke Energy Distinguished Professor in electrical and computer engineering, and also a Founding Faculty Member of the NSF FREEDM Systems Center and the DOE, PowerAmerica Institute. A part of his Ph.D. research on active power filters was commercialized by York Corporation for air-conditioner chillers. His research interests include solid-state transformers, MV power converters, FACTS, utility applications, high-frequency magnetics, and power conversion applications of SiC devices.